

Impact of propagation effects on the spectro-temporal properties of Fast Radio Bursts

AISHWARYA KUMAR ¹, FERESHTEH RAJABI ², AND MARTIN HOUE ¹

¹*Department of Physics and Astronomy, The University of Western Ontario, 1151 Richmond Street, London, Ontario N6A 3K7, Canada*

²*Department of Physics and Astronomy, McMaster University, 1280 Main Street West, Hamilton, Ontario, L8S 4L8, Canada*

ABSTRACT

We present a mathematical analysis of the spectro-temporal properties of Fast Radio Bursts (FRBs), focusing on the distortions introduced by propagation effects such as scattering and inaccurate dedispersion. By examining the impact of different scattering timescales and residual dispersion measures (DMs), both independently and in combination, we identify systematic trends in the sub-burst slope law as defined within the framework of the Triggered Relativistic Dynamical Model (TRDM). These effects primarily alter the measurements of the sub-burst slope and duration, thereby also modifying their correlations with other properties, such as central frequency and bandwidth. Our results show that scatter-induced temporal broadening affects duration more than slope, with weak to moderate scattering subtly modifying the sub-burst slope law and strong scattering causing significant deviations. Residual dispersion preferentially modifies the slope, further changing the trends predicted by the sub-burst slope law. Ultra-short bursts (or ultra-FRBs) emerge as particularly susceptible to these effects even at relatively high frequencies, underscoring the need for precise treatment of scattering and accurate dedispersion before performing analyses. Our findings emphasize the necessity for higher frequency observations (especially for ultra-FRBs) to improve the DM estimates as well as the measurements of spectro-temporal properties.

Keywords: Radio transient sources(2008) — Interstellar scattering(854) — Intergalactic medium(813)
— Analytical mathematics(38) — Computational astronomy(293)

1. INTRODUCTION

Fast Radio Bursts (FRBs) are extraordinarily bright, short-duration transients generally of extragalactic origin. They are typically categorized on the basis of their activity rates into two distinct subtypes: repeating and non-repeating bursts. FRBs exhibit diverse spectro-temporal characteristics, energy distributions, periodicity (for repeating FRBs), and polarization properties. Despite extensive observations, the origins and emission mechanisms of FRBs remain unclear. Establishing correlations between their complex and varied properties serves as a powerful instrument to construe the causation of these events.

As bursts propagate from the source to the observer, their spectro-temporal profiles undergo significant alterations due to propagation effects such as dispersion, scattering, and scintillation. Extracting dispersive delays and scattering timescales is both challenging and crucial, forming the backbone of burst preprocessing and analysis. The underlying dispersion measure (DM) offers insights into the aggregate electron number den-

sity encountered along the path. By employing different methodologies, we are able to measure the DM to a certain degree of precision and detract it using dedispersion techniques. However, inaccuracies in these estimates can lead to residual dispersion in a burst, which affects the measurement of its properties. Scattering, caused by irregularities in the electron density (Scheuer 1968; Rickett 1977; Cordes & Lazio 2002), adds temporal smearing, which is often identified by an exponential tail observed in the frequency-integrated burst profile. Quantifying the scattering timescale poses challenges due to its stochastic nature, which introduces variability in the decay constant governing the tail. To account for scattering, burst profiles are analyzed over time and frequency, necessitating precise dedispersion techniques. Although every burst is subject to dispersion, scattering is observed only in a small subset of sources. Numerous studies have identified and quantified significant scattering components within these sources (Shannon et al. 2018; Ravi 2019; Farah et al. 2019; CHIME/FRB Collaboration et al. 2019; Ocker et al. 2023; CHIME/FRB Collaboration et al. 2023).

Major contributors to the DM include the host galaxy and the local surroundings, the intergalactic medium, and the Milky Way, each imparting electron density to the propagation medium. While these components cumulatively contribute to the DM, they are not entirely predictive of the scattering timescale. In particular, while higher DMs generally suggest longer paths through electron-dense media, thereby implying greater potential for scattering, the actual scattering observed can vary significantly depending on the localized conditions within the intervening media (Cordes & Chatterjee 2019). The intergalactic medium contribution to scattering is generally minimal unless the line of sight intersects electron-dense turbulent structures, such as an intervening galaxy cluster. Studies by Gupta et al. (2022), and Chawla et al. (2022) further highlight decoupling between the estimated DM and scattering timescales of FRBs, suggesting distinct origins for these effects. However, some studies do point towards a moderate correlation (Ravi 2019; CHIME/FRB Collaboration et al. 2019). This dichotomy underlines the diverse environments through which FRBs propagate and the complex dynamics of these events.

This paper investigates the effects of scattering and inaccurate de-dispersion on the spectro-temporal features of FRBs by analyzing deviations in the sub-burst slope law as defined within the framework of the Triggered Relativistic Dynamical Model (TRDM) introduced by Rajabi et al. (2020). We organize our paper in the four sections to follow. Section 2 provides an overview of the TRDM and the sub-burst slope law, and outlines the propagation effects under consideration. In Section 3, we delve into the mathematical formulations used to integrate scattering and DM errors into the evaluation of the sub-burst slope law, providing a perspective on these effects separately and in conjunction. Section 4 presents the results of the spectro-temporal modifications observed in the sub-burst slope law by varying the degree of scattering and residual dispersion. We also explore the behavior of ultra-short FRBs distorted by these effects. Finally, in Section 5, we summarize our findings, detailing the anticipated behavior of bursts under different regimes, and propose strategies to identify and counteract any anomalous behavior observed in the sub-burst slope law.

2. THE SUB-BURST SLOPE LAW AND PROPAGATION EFFECTS

2.1. Triggered Relativistic Dynamical Model (TRDM)

The sub-burst slope law is a characteristic feature of the TRDM where an FRB source is made of different components moving (potentially) at relativistic speeds

relative to the observer. Following a triggering event originating from a background source, each component of the FRB source emits narrowband radiation after a time delay. Due to the relativistic Doppler shift, radiation emitted at a frequency ν' in the source's rest frame is detected at frequency ν in the observer's frame. The finite velocity distribution covered by the components of the FRB source, coupled with the relativistic Doppler shift, transforms the individual narrowband spectra into the wideband emission detected as a sub-burst. Rajabi et al. (2020) expressed the sub-burst slope law¹ as

$$\frac{1}{\nu} \frac{d\nu}{dt_D} = - \left(\frac{\tau'_w}{\tau'_D} \right) \frac{1}{t_w} = - \frac{A}{t_w}, \quad (1)$$

where τ'_D and τ'_w are the delay and duration of the burst in its rest frame. These are related to the delay and duration (t_D and t_w , respectively) in the observer's frame by

$$t_D = \tau'_D \sqrt{\frac{1-\beta}{1+\beta}} = \tau'_D \frac{\nu'}{\nu} \quad (2)$$

$$t_w = \tau'_w \sqrt{\frac{1-\beta}{1+\beta}} = \tau'_w \frac{\nu'}{\nu}. \quad (3)$$

Here, β is the velocity (divided by the speed of light) of the FRB source. Analyses from Rajabi et al. (2020), Chamma et al. (2021), Jahns et al. (2023), Chamma et al. (2023), and Brown et al. (2024) have provided substantial observational support for the relationships given in equations (1) and (3). By leveraging the sub-burst slope law, Chamma et al. (2023) and Brown et al. (2024) derive representative DMs for the sub-bursts. While this method is generally effective, it is important to verify its applicability in the presence of processes like scattering. Furthermore, the sub-burst slope parameter, i.e., A in equation (1), of individual sources can differ from the value obtained when grouping multiple sources together (Brown et al. 2024). Therefore, understanding how spectro-temporal distortions in bursts manifest in the sub-burst slope law is essential.

2.2. Propagation effects

The non-homogeneous distribution of electron density in galaxies leads to sub-bursts having multiple propagation paths, resulting in differential arrival times for

¹ Following the terminology in use in the literature, we refer to a “sub-burst” as a single pulse within an FRB event, which may contain several pulses. The “sub-burst slope law” is defined for sub-bursts, while the “drift law” applies to FRBs containing multiple sub-bursts (Chamma et al. 2021, 2023).

signal components and temporal smearing of the pulse shape. Although this smearing is stochastic and non-linear, it can be quantified by the scattering timescale, τ_{sc} , which depends on the observing frequency, ν , as follows:

$$\tau_{\text{sc}} = \Lambda_{\text{sc}} \left(\frac{\nu}{1 \text{ GHz}} \right)^{-n}, \quad (4)$$

where $n = 4.0$ for the thin screen model and $n = 4.4$ for the Kolmogorov spectrum (Rickett 1977). The constant of proportionality, Λ_{sc} , depends on the scale size of irregularities, a measure of electron density fluctuations, and the distance of the source from the observer. Although we adopt a range of Λ_{sc} from 0 to 20 ms, bursts with scattering timescales outside this range have also been observed (Ravi 2019).

As the pulse travels through different environments, the electron densities present in the source, the intergalactic medium, and the Milky Way introduce dispersion in its spectra. Dispersion is a frequency-dependent delay that causes the lower-frequency components of a sub-burst to arrive later than the higher-frequency counterparts. This time delay, Δt , at frequency ν is expressed as

$$\Delta t = a \text{ DM} \left(\frac{1}{\nu^2} - \frac{1}{\nu_{\text{ref}}^2} \right), \quad (5)$$

where $a = 4.148\,806\,4239(11) \text{ GHz}^2 \text{ cm}^3 \text{ pc}^{-1} \text{ ms}$ (Kulkarni 2020) and ν_{ref} is a reference frequency, typically set to the highest frequency present in a dynamic spectrum or to infinity. For most observed FRBs, the error in DM is usually believed to be on the order of 1% of the reported DM value. For example, FRB 20191221A reported in CHIME/FRB Collaboration et al. (2022) has a DM of 368 pc cm^{-3} with an uncertainty of $\sim 6 \text{ pc cm}^{-3}$. Different studies provide different DM values for the same source, influenced by the timing of observation, the instrumentation used, the specific de-dispersion pipeline employed, and the metric optimized to select the DM (e.g., based on the signal-to-noise ratio (S/N) or the structure of the burst). Chamma et al. (2021, 2023) and Brown et al. (2024) determine the DM for FRB sources by identifying the value that best fits the sub-burst slope law. Most representative DMs calculated through this approach are consistent with those published in other studies. Nevertheless, discrepancies arise for some sources. For example, the reported DM for FRB 20180301A in Price et al. (2019) is $522 \pm 5 \text{ pc cm}^{-3}$. Brown et al. (2024) found that some sub-bursts were over-corrected at this value, resulting in non-physical positive slopes, according to the TRDM. They found the representative DM to be 515.4 pc cm^{-3} ,

resulting in a variance of $\sim 7 \text{ pc cm}^{-3}$. These inconsistencies highlight the ambiguities encountered while ascertaining the DM of the bursts, leading to residual dispersion in samples prepared for analysis.

3. ANALYTICAL FORMULATION OF THE SUB-BURST SLOPE LAW WITH SCATTERING AND RESIDUAL DM

3.1. Scattering-only analysis

In this section, we develop the mathematical framework required to investigate the influence of scattering on the sub-burst slope law. We initiate our analysis by considering a sub-burst of duration t_w . The intensity of the sub-burst is modeled with a decaying exponential profile, expressed as:

$$I_1(\nu, t) = \frac{F_0}{t_w} \exp \left[-\frac{(t - t_D)}{t_w} \right] H(t - t_D), \quad (6)$$

where $H(t)$ is the Heaviside distribution. In this equation, F_0 represents the fluence, and t_D is the intrinsic delay at frequency ν of the sub-burst, as previously described in equation (2). We model scattering as a one-sided exponential function based on the thin screen approximation (Cronyn 1970; Rickett 1977; Jankowski et al. 2023) as follows:

$$S(\nu, t) = \frac{1}{\tau_{\text{sc}}} \exp \left(\frac{-t}{\tau_{\text{sc}}} \right) H(t), \quad (7)$$

where the scattering timescale, τ_{sc} , is given in equation (4). The post-scattering sub-burst profile, obtained by convolving the intensity profile with the scattering function, is given by:

$$I(\nu, t) = I_1(\nu, t) * S(\nu, t). \quad (8)$$

Equation (8) can be calculated to be

$$I(\nu, t) = \frac{F_0}{\tau_{\text{sc}} - t_w} \left\{ \exp \left[\frac{-(t - t_D)}{\tau_{\text{sc}}} \right] - \exp \left[\frac{-(t - t_D)}{t_w} \right] \right\} H(t - t_D). \quad (9)$$

To lighten the notation we will, from now on, omit the Heaviside distribution $H(t - t_D)$ with the understanding that the signal is 0 for $t < t_D$. We also find that the timescale of this function comes out to be

$$\begin{aligned} \lambda &= \int_{t_D}^{\infty} \frac{t - t_D}{\tau_{\text{sc}} - t_w} \left\{ \exp \left(\frac{-(t - t_D)}{\tau_{\text{sc}}} \right) - \exp \left(\frac{-(t - t_D)}{t_w} \right) \right\} dt \\ &= \tau_{\text{sc}} + t_w. \end{aligned} \quad (10)$$

Here, λ is a function of frequency reflecting the dependence of both t_w and τ_{sc} on ν (as per equations (3) and (4)). To simplify our analysis, we introduce a change of variables as follows

$$(\tau_{sc}, t_w) \rightarrow (\lambda = \tau_{sc} + t_w, T = \tau_{sc} - t_w), \quad (11)$$

which leads to a modified intensity profile of the sub-burst:

$$I(\nu, t) = \frac{F_0}{T} \left\{ \exp \left[\frac{-2(t - t_D)}{\lambda + T} \right] - \exp \left[\frac{-2(t - t_D)}{\lambda - T} \right] \right\}. \quad (12)$$

For clarity, we distinguish each exponential in the intensity profile as distinct standalone functions,

$$h_1(\nu, t) = \frac{F_0}{T} \exp \left[\frac{-2(t - t_D)}{\lambda + T} \right] \quad (13)$$

$$h_2(\nu, t) = \frac{F_0}{T} \exp \left[\frac{-2(t - t_D)}{\lambda - T} \right] \quad (14)$$

such that

$$I(\nu, t) = h_1(\nu, t) - h_2(\nu, t). \quad (15)$$

Now that we have a function for the intensity of a scattered sub-burst, we can use it to evaluate the normalized sub-burst slope law as follows:

$$\frac{1}{\nu} \frac{\partial \nu}{\partial t_D} = \frac{1}{\nu} \frac{\partial \nu}{\partial I(\nu, t)} \frac{\partial I(\nu, t)}{\partial t_D}. \quad (16)$$

Performing an average of equation (16) over the extent of the signal allows us to evaluate the mean frequency normalized sub-burst slope as

$$\begin{aligned} \left\langle \frac{1}{\nu} \frac{\partial \nu}{\partial t_D} \right\rangle &= -\frac{1}{\Delta \nu} \int_{\nu - \Delta \nu / 2}^{\nu + \Delta \nu / 2} d\nu \int_0^\infty dx \\ &\quad \times \frac{T}{\Delta} \left[\lambda (h_1 - h_2)^2 - T (h_1^2 - h_2^2) \right], \end{aligned} \quad (17)$$

with

$$\begin{aligned} \Delta &= T [h_1(\lambda - T)(nx + t_D) - h_2(\lambda + T)(x + t_D)] \\ &\quad - (h_1 - h_2) \left(\frac{\lambda^2 - T^2}{4} \right) [(n-1)\lambda + (n+1)T], \end{aligned} \quad (18)$$

where $x = t - t_D$, $h_i = h_i(\nu, x)$ ($i = 1, 2$), $T = T(\nu)$, $\lambda = \lambda(\nu)$ and $\Delta \nu$ is the frequency extent of the signal. The sub-burst duration at its central frequency, λ_c , as defined in equation (10), will be used to plot the sub-burst slope law in the presence of scattering.

When contrasting the scattering timescale with the sub-burst duration, two limiting cases are of particular importance to our analysis. The first case corresponds to the scenario where the scattering timescale is much smaller than the duration ($\tau_{sc} \ll t_w$). In this weak scattering regime, we have $\lambda \simeq -T \simeq t_w$ and $h_1 \ll h_2$. Substituting these in equations (17) and (18) and utilizing pertinent approximations (e.g., $\Delta \nu \ll \nu$), we solve the integral analytically to arrive at

$$\begin{aligned} \left\langle \frac{1}{\nu} \frac{\partial \nu}{\partial t_D} \right\rangle &\simeq \exp \left(\frac{1}{A} - 1 \right) \text{E}_i \left(1 - \frac{1}{A} \right) \frac{1}{t_{w,c}} \\ &\simeq -\frac{A}{t_{w,c}} \end{aligned} \quad (19)$$

for the sub-burst slope law, where $\text{E}_i(x)$ is the exponential integral, A is defined in equation (1) and $t_{w,c}$ is the duration at the center frequency of the sub-burst (i.e., evaluated from equation 3). This form is analogous to equation (1) indicating that weakly scattered bursts adhere closely to the ideal sub-burst slope law.

The second regime is when $\tau_{sc} \gg t_w$ and scattering becomes dominant. Here, $\lambda \simeq T \simeq \tau_{sc}$, $h_1 \gg h_2$ and the approximate slope law becomes

$$\begin{aligned} \left\langle \frac{1}{\nu} \frac{\partial \nu}{\partial t_D} \right\rangle &\simeq \frac{\exp(-1) \text{E}_i(1)}{n \tau_{sc,c}} \\ &\simeq \frac{0.16}{\tau_{sc,c}}, \end{aligned} \quad (20)$$

where $\tau_{sc,c}$ is the value of the scattering timescale at the center frequency (from equation 4) and we used $n = 4$ for the last relation (as well as $\Delta \nu \ll \nu$). In this regime, the slope becomes positive, implying that high levels of scattering in a sub-burst invert the slope to positive values. As the scattering timescale is frequency dependent, sub-bursts at lower frequencies are more significantly affected even at shorter scattering timescales. Based on this, we should observe a transition from negative to positive slope as the central frequency of the sub-burst decreases, with this transition occurring at progressively higher frequencies as the scattering timescale increases. We caution that the approximate solutions presented in equations (19) and (20) are not complete solutions but are only valid in the corresponding limits. They do, however, inform us on what to expect for the underlying behavior of the sub-burst slope law as the level of scattering increases. That is, and we will see later on, a change of sign in the sub-burst slope manifests itself strikingly in the appearance of the law.

There is a third regime where $\tau_{sc} \simeq t_w$ for which such approximations are infeasible. For a thorough investigation in all three regimes, the integral specified

in equation (17) must be solved numerically to investigate the complexities introduced by scattering. It is, however, difficult to obtain a numerical solution, as the wide domain of integration challenges the limits of computational precision. To counteract this shortcoming, we employ techniques to identify the critical points and adapt the integration domain accordingly. Additionally, we utilize a Savitzky–Golay filter to smooth the sub-burst slope obtained post-integration, to reveal broader trends in the relationship in the figures to follow.

3.2. DM-only analysis

To begin, we define the frequency-dependent residual dispersive delay in a sub-burst at central frequency ν as

$$\Delta t_{\text{DM}} = a \Delta \text{DM} \left(\frac{1}{\nu^2} - \frac{1}{\nu_{\text{ref}}^2} \right) \text{ ms} \quad (21)$$

following equation (5). In subsequent analysis, ΔDM refers to the residual DM left in the source after de-dispersion. That is,

$$\Delta \text{DM} = \text{DM}_{\text{true}} - \text{DM}_{\text{est}}, \quad (22)$$

where DM_{true} is the actual dispersion present in the source spectra and DM_{est} denotes the estimated DM using a specific method or analysis. Thus, the value of $\Delta \text{DM} = 0 \text{ pc cm}^{-3}$ is indicative of perfect de-dispersion or the absence of residual dispersion in a sub-burst. A positive $\Delta \text{DM} (> 0 \text{ pc cm}^{-3})$ implies under-dedispersion and a negative $\Delta \text{DM} (< 0 \text{ pc cm}^{-3})$ corresponds to the case of over-dedispersion.

To evaluate the delay in each channel, we are free to set $\nu_{\text{ref}} \rightarrow \infty$ in equation (21). We thus define our intensity function as

$$I_2(\nu, t) = \frac{F_0}{t_w} \exp \left[\frac{-(t - t_{\text{D}}^*)}{t_w} \right], \quad (23)$$

where the new delay, t_{D}^* , is due to the intrinsic delay introduced by the model (t_{D}), and the delay due to dispersion (Δt_{DM}), i.e., $t_{\text{D}}^* = t_{\text{D}} + \Delta t_{\text{DM}}$. To streamline the expression, we have omitted the Heaviside function $H(t - t_{\text{D}}^*)$ from equation (23), still with the understanding that the signal intensity is zero for $t < t_{\text{D}}^*$. The normalized sub-burst slope law becomes

$$\frac{1}{\nu} \frac{\partial \nu}{\partial t_{\text{D}}^*} = \frac{1}{\nu} \frac{\partial \nu}{\partial I_2(\nu, t)} \frac{\partial I_2(\nu, t)}{\partial t_{\text{D}}^*}. \quad (24)$$

Solving the partial derivatives, we arrive at the frequency normalized sub-burst slope law

$$\left\langle \frac{1}{\nu} \frac{\partial \nu}{\partial t_{\text{D}}^*} \right\rangle = \frac{1}{\Delta \nu} \int_{\nu - \Delta \nu/2}^{\nu + \Delta \nu/2} d\nu \times \frac{1}{t_w} \int_0^\infty dx \frac{\exp(-x/t_w)}{t_w - x - t_{\text{D}}^* - \Delta t_{\text{DM}}} \quad (25)$$

with $x = t - t_{\text{D}}^*$. The sub-burst duration is given by

$$\lambda = \int_{t_{\text{D}}^*}^\infty \frac{(t - t_{\text{D}}^*)}{t_w} \left\{ \exp \left[\frac{-(t - t_{\text{D}}^*)}{t_w} \right] \right\} dt = t_w. \quad (26)$$

We perform a numerical integration of equation (25) and use equation (26) to calculate the duration at central frequency ($\lambda_c = t_{w,c}$) to plot the sub-burst slope law. The results are presented in section 4.2.

Using the exponential integral $E_i(x)$ and its properties, the temporal integral equation (25) can be approximated to the following,

$$\left\langle \frac{1}{\nu} \frac{\partial \nu}{\partial t_{\text{D}}^*} \right\rangle \simeq -\frac{A}{t_{w,c}} \left[1 - \frac{\Delta \text{DM}}{\Delta \text{DM} + A_1 \nu / (2Aa)} \right] \quad (27)$$

whenever $-\Delta \text{DM} \ll A_1 \nu / (2Aa)$ and $\Delta \nu \ll \nu$. As before, $t_{w,c}$ is the sub-burst duration at the center frequency while we used the relativistic invariant $A_1 = \nu t_{w,c}$. This solution shows that the original sub-burst slope law (equation (1)) is recovered for minimal residual dispersion, as expected, while an error term due to ΔDM is added otherwise. As can be intuitively asserted, this relation makes it clear that under-dedispersion ($\Delta \text{DM} > 0$) flattens the slope and over-dedispersion ($-A_1 \nu / (2Aa) \ll \Delta \text{DM} < 0$) accentuates it. Although lying beyond its domain of applicability, we note that equation (27) also suggests that, as was the case for the scattering-dominated approximation, the normalized sub-burst slope will change sign when excessive over-dedispersion is present (i.e., $\Delta \text{DM} \ll -A_1 \nu / (2Aa) < 0$). As we will soon see, this will again drastically alter the shape and behavior of the sub-burst slope law.

3.3. All-inclusive analysis

We now combine the analysis described in Sections 3.1 and 3.2 to evaluate the sub-burst slope trend in the presence of both scattering and residual DM. The consolidated intensity profile, following the convolution derived in equation (9) and adjusted to include the modified delay term (t_{D}^*) introduced in Section 3.2, is given by:

$$I(\nu, t) = \frac{F_0}{T} \left\{ \exp \left[\frac{-2(t - t_{\text{D}}^*)}{\lambda + T} \right] - \exp \left[\frac{-2(t - t_{\text{D}}^*)}{\lambda - T} \right] \right\} \quad (28)$$

where λ and T are defined in equation (11). Notice that the Heaviside function is again dropped for simplicity. We follow the same mathematical treatment outlined in previous sections (3.1 and 3.2) to obtain the expression for the normalized sub-burst slope law as

$$\left\langle \frac{1}{\nu} \frac{\partial \nu}{\partial t_D^*} \right\rangle = -\frac{1}{\Delta \nu} \int_{\nu-\Delta\nu/2}^{\nu+\Delta\nu/2} d\nu \int_0^\infty dx \times \frac{T}{\Delta} \left[\lambda (h_1 - h_2)^2 - T (h_1^2 - h_2^2) \right], \quad (29)$$

with

$$\begin{aligned} \Delta = & T [h_1 (\lambda - T) (nx + t_D^* + \Delta t_{DM}) \\ & - h_2 (\lambda + T) (x + t_D^* + \Delta t_{DM})] \\ & - (h_1 - h_2) \left(\frac{\lambda^2 - T^2}{4} \right) [(n-1)\lambda + (n+1)T], \end{aligned} \quad (30)$$

where, as before, $x = t - t_D^*$, $h_i = h_i(\nu, x)$ ($i = 1, 2$), $T = T(\nu)$, and $\lambda = \lambda(\nu)$. The timescale of emission, λ_c , evaluated at sub-burst's central frequency is the same as equation (32) with t_D^* substituted for t_D . The complexity of this integral makes it unfeasible to seek an analytical solution or approximation. We rely on numerical methods to obtain a solution, while addressing the critical regions where the function exhibits problematic behavior (as stated at the end of section 3.1).

4. RESULTS AND DISCUSSION

Here, we present the results of the numerical integration performed for the three cases discussed in the previous sections: scattering-only, residual DM-only, and the combined effects of scattering and residual DM. In the observational literature, the sub-burst slope law has been tested extensively for bursts emanating from FRB 20121102A. Studies by Rajabi et al. (2020), Jahns et al. (2023), and Chamma et al. (2023) demonstrate an inverse relationship of slope with duration of the type At_w^{-1} , as presented in equation (1). The constant A was found to lie between 0.07 and 0.1. This finding is corroborated by Chamma et al. (2021) and Brown et al. (2024), where a similar range for A is reported across multiple sources. This consistency reinforces the notion that the parameter A represents an intrinsic property of the FRB source and/or the physical process responsible for the emission of radiation. We conducted our analysis for $0.07 \leq A \leq 0.2$ and since these values demonstrated similar trends, we select $A = 0.1$ for all our subsequent plots. The aforementioned studies also note a relation between the observed duration and central frequency which varies as $t_w \approx 1.5(\text{ms} \cdot \text{GHz})/\nu$ (Brown et al. 2024). For the first part of our analysis, we adopted this value to correlate the sub-burst's duration and delay, through equations (2) and (3), while we reduced it when considering ultra-FRBs in Sec. 4.4. Following the

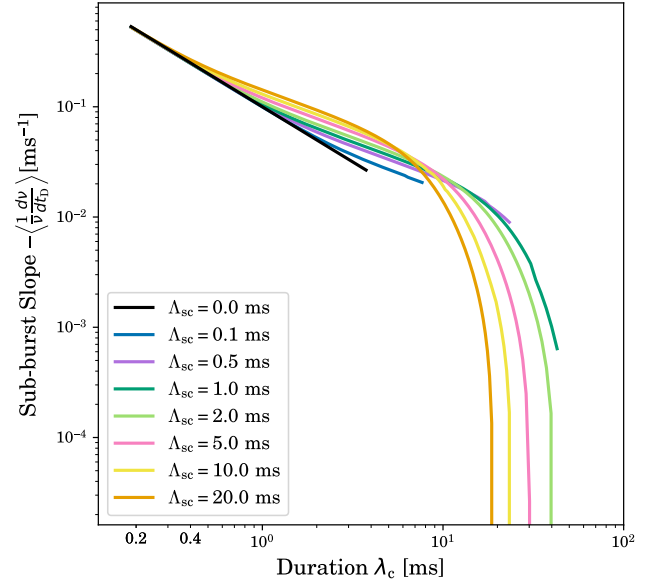


Figure 1. The relationship between the (negative of the) normalized sub-burst slope and the duration ($\lambda_c = \tau_{sc,c} + t_{w,c}$) at the center frequency for different values of scattering timescales (Λ_{sc}). The black line shows the ideal behavior without scattering as per the TRDM of Rajabi et al. (2020). The different colored lines correspond to varying scattering timescales, evaluated using our methods presented in section 3.1. Note that the negative of the sub-burst slope is plotted, as it is typically negative and would otherwise not be visible on a log-scaled axis. In doing so, the slightly positive values of the slope at larger scattering timescales are omitted (see Fig. 2).

findings of Houde et al. (2019), Chamma et al. (2023) and Brown et al. (2024), the bandwidth of the sub-burst is set to $B_\nu = 0.14 \nu$ (GHz), where ν is the observed central frequency of the sub-bursts. For our simulations, ν is in the range of 0.4 GHz to 8 GHz. Additionally, we have chosen a scattering index of $n = 4.0$, although simulations with $n = 4.4$ for the Kolmogorov spectrum also yield similar outcomes.

We would like to emphasize that we plot the negative of the sub-burst slope in all our figures. This approach allows for effective visualization of the sub-burst slope across a wide range of frequencies and durations using logarithmic scales (i.e., the sub-burst slope is intrinsically negative). However, as discussed in the forthcoming sections, there are instances where the slope becomes positive due to excessive scattering and/or residual dispersion. In such cases, these positive values are omitted from the plots due to the logarithmic scaling of the axes. The change in sign of the sub-burst slope is illustrated in Figure 2 for the scattering-only case.

4.1. Effects of scattering on the sub-burst slope law

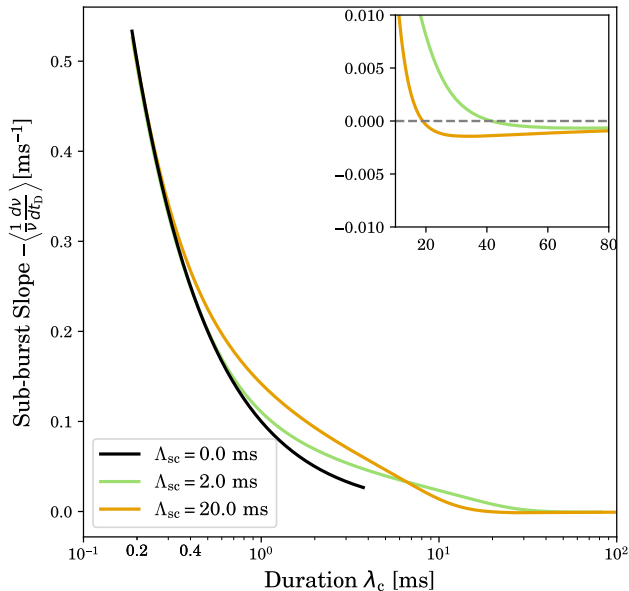


Figure 2. Same as Figure 1 but using a linear scale for the vertical axis. The inset plot captures the transition to positive sub-burst slope values at durations greater than approximately 10 ms that are not visible in Fig. 1. Notice that the transition occurs earlier, at approximately 20 ms, when $\Lambda_{\text{sc}} = 20$ ms as compared to 40 ms for curve with $\Lambda_{\text{sc}} = 2$ ms.

In order to evaluate the sub-burst slope under varying scattering conditions, we perform computations across eight different scattering timescales, including the scenario of no scattering ($\tau_{\text{sc}} = 0$ ms).

4.1.1. Sub-burst slope vs. duration

As our focus is on scattering, we assume that our sub-bursts are devoid of any residual dispersive effects. Figure 1 presents the (negative of the) center frequency normalized sub-burst slope law for various scattering timescales, as computed in equation (17). The conventional law without scattering is represented by the solid black line, where the sub-burst slope is simply $-A/t_w$, with $A = 0.1$. Note that $0.19 \text{ ms} \lesssim t_w \leq 3.75 \text{ ms}$ for the chosen parameters. This curve serves as a baseline for comparison amongst different scattering timescales. We observe that for all scattering timescales, the sub-burst slope flattens out as the duration increases, while a significant drop in slope is observed at longer durations for higher scattering timescales.

At durations less than 0.4 ms, the scattered and the unscattered curves overlap, indicating that the scattered system adheres closely to the predicted TRDM law, thus affirming the validity of the approximations presented in equation (19). This regime corresponds to the scenario where the scattering timescale, τ_{sc} , is significantly shorter than the intrinsic duration, i.e., $\tau_{\text{sc}} \ll t_w$. As the

level of scattering (Λ_{sc}) increases, the observed duration of the sub-burst begins to stretch out for a given slope value, since $\lambda = \tau_{\text{sc}} + t_w$. For instance, the sub-burst with the longest initial duration (3.75 ms) in the unscattered case extends to approximately 8 ms and shows a subtle reduction in slope when $\Lambda_{\text{sc}} = 0.1$ ms. As Λ_{sc} increases incrementally, the effects of temporal broadening and sub-burst slope reduction become progressively more pronounced. With duration increasing disproportionately relative to the reduction in the sub-burst slope, the curves begin to plateau within the 1–10 ms range. For durations beyond 10 ms, the slope decreases by more than two orders of magnitude for all $\Lambda_{\text{sc}} \geq 2.0$ ms. At such high scattering timescales, where $t_w \ll \tau_{\text{sc}}$, the temporal profile may become sufficiently distorted that the slope changes sign, becoming positive. This is indicative of the regime described by equation (20), where scattering dominates. This abrupt decline in slope occurs at earlier stages for higher values of Λ_{sc} . To better visualize these effects, we present the (negative of) the sub-burst slope plotted against duration in Figure 2 using a linearly scaled axis for the sub-burst slope. A transition to negative values (implying positive sub-burst slope) is clearly visible in the inset.

4.1.2. Sub-burst slope vs. frequency

If we combine equations (1) and (3) for the ideal unscattered case, we find that the normalized sub-burst slope varies with the observing frequency as

$$\frac{1}{\nu} \frac{d\nu}{dt_D} = -\frac{A\nu}{\tau_w' \nu'} = -A_2 \nu, \quad (31)$$

where $A_2 = A/\tau_w' \nu' = 1/\tau_D' \nu'$ is a relativistic invariant. This law is denoted by the black solid line in Figure 3 which plots (negative of) the sub-burst slope against the central frequency of the sub-burst. The frequency dependent behavior of scattering is immediately evident from this figure. At higher frequencies ($\nu \gtrsim 4.0$ GHz) all curves align closely with the ideal, unscattered case. This is due to the ν^{-n} dependence of scattering on frequency ($n = 4$ for our calculations; see equation 4), which renders high-frequency sub-bursts less susceptible to temporal distortion caused by irregularities in the propagation medium. In contrast, the curves at lower frequencies ($\nu \lesssim 4.0$, GHz) exhibit clear deviations from the ideal behavior, as low-frequency sub-bursts interact more strongly with the medium. The slope values drop by more than two orders of magnitude (for $\Lambda_{\text{sc}} \geq 2$ ms at frequencies below ~ 2 GHz) depending on amount of scattering present in the sub-bursts. The curves with negligible amounts of scattering ($\Lambda_{\text{sc}} = 0.1, 0.5$ ms) only deviate slightly from the ideal black line for central frequencies less than ~ 600 MHz.

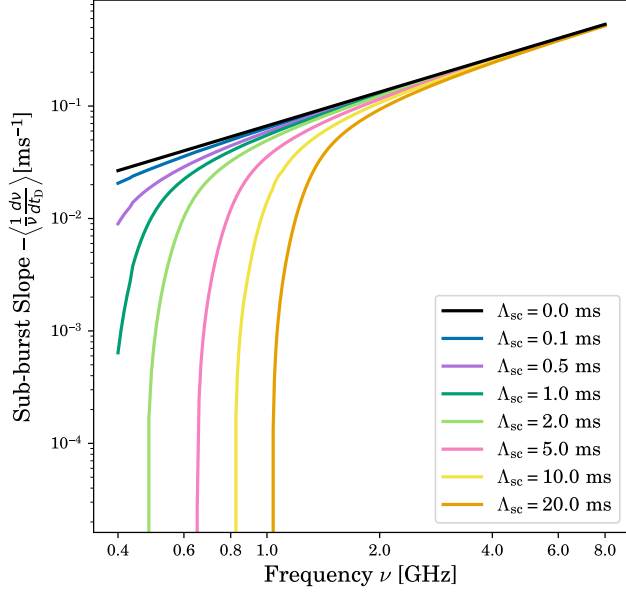


Figure 3. The (negative of the) normalized sub-burst slope against the observed central frequency in range of 0.4 GHz to 8 GHz for different scattering timescales (Λ_{sc}). The solid black line corresponds to the ideal law derived using the TRDM for $\Lambda_{sc} = 0$ ms (Rajabi et al. 2020). Distinct scattering timescales are shown by colored lines.

4.1.3. Other spectro-temporal correlations

In Figure 4, we present the relationship between the center frequency (top panel) and bandwidth (bottom panel) of a sub-burst with its duration. Equation (3) predicts an inverse relationship between the sub-burst duration and the observed frequency, a trend consistent with findings from several studies such as Gajjar et al. (2018) (see their Fig. 7), Chamma et al. (2023) (their Fig. 4) and Brown et al. (2024) (their Fig. 2). In our figure, this relationship is represented by a solid black line. However, deviations from the inverse relationship are apparent in the presence of scattering since the curves shown in the figure are obtained from equations (3)-(4). We then express the total duration as a function of frequency as:

$$\lambda = \frac{A_1}{\nu} + \Lambda_{sc} \left(\frac{1 \text{ GHz}}{\nu} \right)^n, \quad (32)$$

with, as before, $A_1 = \nu' \tau_w'$ (a relativistic invariant).

We can clearly identify the two limiting behaviors. At lower frequencies, where $\nu^{n-1} \ll \Lambda_{sc}/A_1$ (i.e., $t_w \ll \tau_{sc}$), equation (32) approximates $\lambda \sim \Lambda_{sc} (1 \text{ GHz}/\nu)^n$ and the curves shift rapidly toward longer durations, as seen in the top panel of Figure 4. On the other hand, when $\nu^{n-1} \gg \Lambda_{sc}/A_1$ (i.e., $t_w \gg \tau_{sc}$), the duration converges to the other limit, where $\lambda \sim A_1/\nu$ and the curves corresponding to different values of Λ_{sc} approach

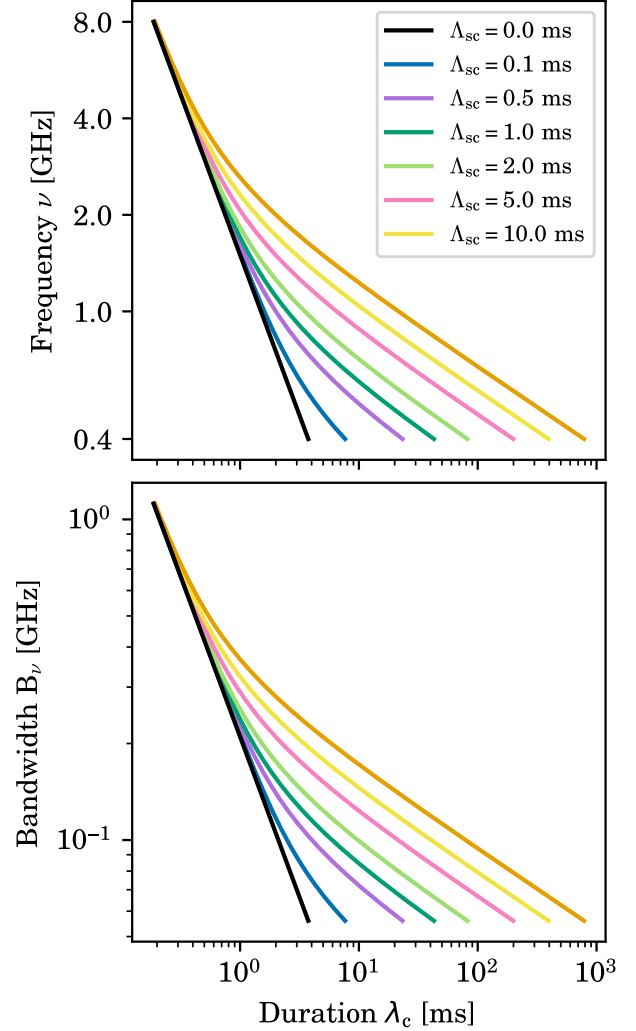


Figure 4. Relationship between the observed duration and center frequencies of sub-bursts (top) and between bandwidth and duration (bottom). In both plots, the solid black line represents the ideal relationship as predicted by the TRDM (Rajabi et al. 2020). The different scattering timescales (Λ_{sc}) are color coded according to the legend, while the duration at center frequency λ_c is calculated using equation (32) and the bandwidth is set to $B_\nu = 0.14\nu$.

the unscattered case. Deviation from the ideal inverse trend is observed in some published data. For example, in Chamma et al. (2023) the free-parameter fit for FRB 121102A presented in their Figure 4 yields $\lambda \propto \nu^{-1.77}$ over $1 \text{ GHz} \lesssim \nu \lesssim 6 \text{ GHz}$ but with deviations from the ideal $\propto \nu^{-1}$ relation most evident at the low-frequency end of that range. Such results can be used as a tool to evaluate the scattering timescale of a source. Acquiring data across different frequencies for the same source is essential for any such determination.

The expected relationship between bandwidth and duration according to the TRDM follows the form $B_\nu \propto \lambda^{-1}$, based on the proportionality $t_w \propto \nu^{-1}$ and the observed relation $B_\nu \propto \nu$ (Houde et al. 2019; Rajabi et al. 2020; Chamma et al. 2023; Bethapudi et al. 2023; Brown et al. 2024), which is forced in our analysis. While it is found that this behavior is generally consistent across different sources, Chamma et al. (2023) and Brown et al. (2024) suggest that a relationship of the form $B_\nu \propto \lambda^{-1/2}$ may agree better with observational data. We can see, however, that this deviation from the expected relationship is readily explained by incorporating the effects of scattering, as presented in Figure 4 (bottom panel). In the figure, the curve for unscattered sub-bursts (black line) represents the λ_c^{-1} relationship between the bandwidth and duration as predicted by the TRDM. This relationship generally holds well at shorter durations (< 1 ms), or equivalently, at higher frequencies and larger bandwidths, across curves with varying levels of scattering. However, sub-bursts with narrower bandwidths (and thus lower frequencies) have their temporal profiles smeared with scattering, resulting in a shallower relationship.

4.2. Effects of residual dispersion on the sub-burst slope law

In this section, we numerically solve the integral in equation (25) to evaluate the slope at different central frequencies for sub-bursts with residual dispersion (ΔDM) ranging from -5.0 to $+5.0$ pc cm^{-3} . The results are presented in Figure 5, showing the sub-burst slope against its duration (note that here, $\tau_{\text{sc}} = 0$ and, therefore, $\lambda = t_w$). Overall, over-dedispersion ($\Delta\text{DM} < 0$) results in steeper, more vertical burst profiles, leading to steeper slopes. On the other hand, under-dedispersion ($\Delta\text{DM} > 0$) produces shallower slopes. We also examine the sub-burst slope as a function of frequency in Figure 6. The inverse square dependence of DM on frequency, which disproportionately affects lower frequencies is very apparent from this figure. When examined together, Figures 5 and 6 provide a comprehensive view of how residual dispersion influences the spectro-temporal behavior of the sub-burst slope law.

Observational data indicate that small variations in the DM value chosen for dedispersion affect the sub-burst slope law by shifting the fit vertically in the figures (i.e., changing the value of the constant A) while approximately preserving the inverse relationship (see Figure 3 of Chamma et al. 2023). This feature is encapsulated in Equation (27), which introduces an additional term contingent on the residual DM. As mentioned earlier (Section 3.2), over-dedispersion ($\Delta\text{DM} < 0$) increases

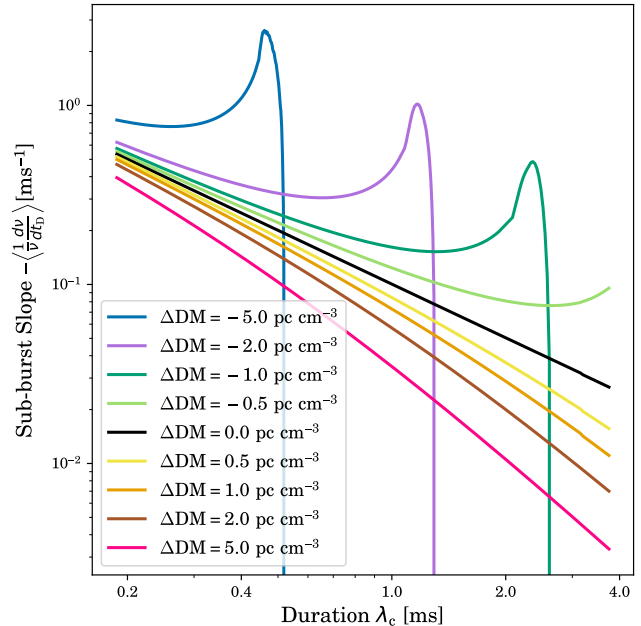


Figure 5. Sub-burst slope vs. sub-burst duration for various dispersion measures in the range of -5.0 pc cm^{-3} to 5.0 pc cm^{-3} . The black line corresponds to the undispersed case that follows the ideal law as described by the TRDM. For all curves, $\tau_{\text{sc}} = 0$, and therefore, $\lambda_c = t_{w,c}$.

the value of the parameter A , while under-dedispersion decreases it. This explains why the curves separate according to ΔDM at shorter durations (≈ 0.2 ms) or higher frequencies (≈ 8 GHz) in Figures 5 and 6, respectively. That is, over-dedispersed curves lie above the undispersed case (solid black line), while the under-dedispersed curves fall below.

As discussed at the end of Sec. 3.2, when the applied (over-)dedispersion is too strong, the lower-frequency components of the burst progressively catch up with the higher-frequency ones, creating an artificially compressed and steeper waterfall, and eventually changing the sign of its slope. Therefore, in Figure 5, curves with over-dedispersion see their normalized sub-burst slope increase before drastically falling to much lower values. For instance, the curve for $\Delta\text{DM} = -5.0$ pc cm^{-3} reaches a peak slope value of ≈ 3 ms^{-1} , compared to ≈ 0.2 ms^{-1} for the undispersed case $\Delta\text{DM} = 0$ pc cm^{-3} at the same position, before collapsing at duration ≈ 0.5 ms. Similar to the case of scattering discussed in Sec. 4.1.1, this behavior corresponds to a transition to positive slopes, which are considered non-physical under the framework of the TRDM and are not visible on our log-log plot. The effect is more pronounced and happens at shorter durations with increasing over-dedispersion.

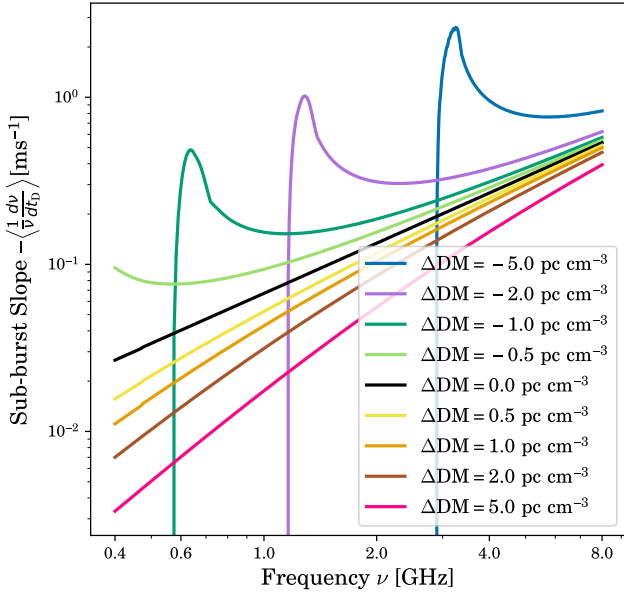


Figure 6. The frequency-normalized sub-burst slope vs. frequency for ΔDM in the range of -5.0 pc cm^{-3} to 5.0 pc cm^{-3} . Different colors represent different dispersion measure values, while the black line represents sub-bursts with no residual dispersion.

The same behavior in the normalized sub-burst slope law is shown in Figure 6, but as a function of the central frequency. We observe that even at high frequencies (8 GHz), the slopes deviate from the undispersed case. As frequency decreases, the effect of residual dispersion becomes more pronounced due its ν^{-2} dependence, causing the sub-burst profiles to steepen and the slopes to rise. Below a critical frequency, over-dedispersion ($\Delta\text{DM} < 0 \text{ pc cm}^{-3}$) causes a change in the sign of the sub-burst slope, as evidenced by its sharp decline during this transition. The higher the over-dedispersion (i.e., the more negative ΔDM value), the higher the frequency at which this transition occurs.

Under-dedispersed sub-bursts, which result from insufficient DM correction (i.e., when $\Delta\text{DM} > 0$), exhibit shallower waterfall slopes. As a consequence, and as mentioned earlier, the corresponding curves in Figures 5 and 6 lie below the undispersed case. As the duration increases (and the frequency decreases), these curves deviate further from the ideal sub-burst slope law. The higher the value of ΔDM , the more pronounced the effect.

As evidenced by our figures, the deviation from the ideal law remains marginal at frequencies above 1 GHz for $-1 \text{ pc cm}^{-3} \leq \Delta\text{DM} \leq 1 \text{ pc cm}^{-3}$. The true extent of any deviation, however, is contingent upon the frequency range of the sub-bursts considered and the magnitude of ΔDM .

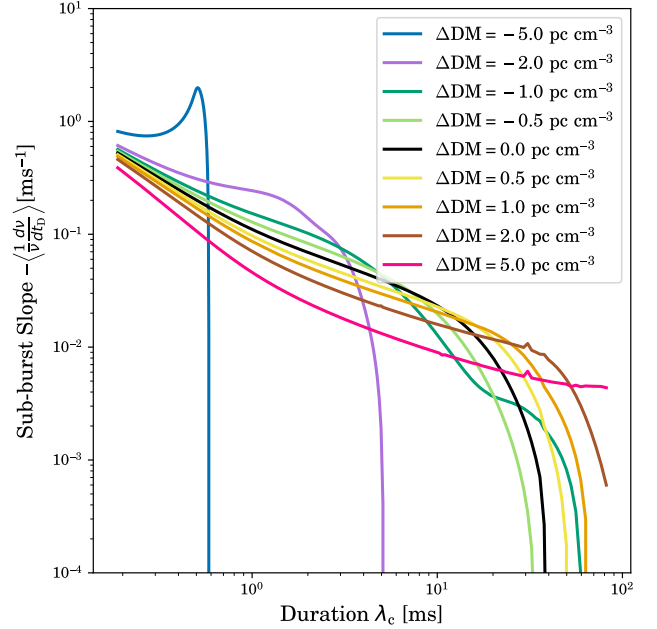


Figure 7. The frequency-normalized sub-burst slope against the duration for $-5.0 \text{ pc cm}^{-3} \leq \Delta\text{DM} \leq +5.0 \text{ pc cm}^{-3}$ and a fixed scattering timescale $\Lambda_{\text{sc}} = 2 \text{ ms}$. The trends illustrate the complex interplay between these two effects: negative ΔDM s tend to force the curve upwards, while scattering pushes it downwards, resulting in an erratic shape. For positive ΔDM s, both processes work in conjunction, yielding a lower slope.

4.3. Combined effects of scattering and dispersion on the sub-burst slope law

Having examined the effects of scattering and dispersion independently, we now investigate their combined impact on the sub-burst slope law. We select the scattering timescale of $\Lambda_{\text{sc}} = 2.0 \text{ ms}$ and conduct our computations for $-5.0 \text{ pc cm}^{-3} \leq \Delta\text{DM} \leq +5.0 \text{ pc cm}^{-3}$.

Figures 7 and 8 depict the frequency-normalized sub-burst slope trend as a function of the duration and frequency, respectively, across our chosen ΔDM range. From our previous analysis, we know that scattering causes a reduction in the sub-burst slope as the duration increases and frequency decreases (see Figs. 1 and 3). Residual dispersion, on the other hand, affects the slopes differently based on its magnitude and type (under-dedispersion or over-dedispersion; see Figs. 5 and 6). In Figures 7 and 8 we observe complex curve profiles, particularly for over-dedispersed sub-bursts. To better understand the characteristics of the sub-burst slope law under the combined effects of scattering and residual dispersion we divide our analysis based on the type and degree of residual dispersion in the system.

Severe over-dedispersion. Sub-bursts with $\Delta\text{DM} = -5.0 \text{ pc cm}^{-3}$ exhibit slopes predominantly

shaped by residual dispersion, while scattering effects remain negligible. The curves remain virtually identical to the residual dispersion case shown in Figures 5 and 6. The transition to positive slopes occurs at shorter durations (~ 0.6 ms) or at relatively higher frequencies (~ 3 GHz).

Moderate over-dedispersion. For sub-bursts with $\Delta\text{DM} = -2.0$ pc cm^{-3} and -1.0 pc cm^{-3} both scattering and residual dispersion affect the sub-burst slope. The latter steepens the sub-burst slope while scattering tends to flatten it (until the sub-bursts exhibit a change of sign in their slope) leading to distorted curves. In Figures 7 and 8 we observe an attenuated bump and a decline that is shifted towards longer duration and lower frequencies due to scattering (when compared with Figures 5 and 6). However, the decline in sub-burst slope for $\Delta\text{DM} = -2.0$ pc cm^{-3} curve is still affected primarily by residual dispersion. In case of $\Delta\text{DM} = -1.0$ pc cm^{-3} , the competing effects of scattering and dispersion shape the behavior for $10 \text{ ms} \lesssim \lambda_c \lesssim 60 \text{ ms}$ (or $0.4 \text{ GHz} \lesssim \nu \lesssim 1 \text{ GHz}$), with scattering eventually dominating and driving the decline towards longer duration and lower frequencies.

Weak over-dedispersion. For $\Delta\text{DM} = -0.5$ pc cm^{-3} , scattering dominates, leading to a typical reduction in sub-burst slope as the duration increases and the frequency decreases. However, mild residual dispersion causes the sub-burst slope to change sign earlier, around 30 ms, compared to 40 ms in the undispersed case (black curve).

Weak under-dedispersion. For ΔDM in range of 0.5 pc cm^{-3} to 2.0 pc cm^{-3} , the sub-burst slopes are only slightly reduced from the undispersed case (black curve) at shorter durations (< 10 ms). As under-dedispersion flattens the sub-burst slope, the curves begin with shallow slope values at higher frequencies and shorter durations. The slope gradually decreases as the influence of scattering increases and changes sign (after ~ 50 ms).

Moderate to severe under-dedispersion. For $\Delta\text{DM} = 5.0$ pc cm^{-3} , shallow sub-burst slopes are observed at shorter durations (< 1 ms) and higher frequencies (8.0 GHz). Scattering has minimal impact on the already shallow slopes, leading to a gradual decline as duration increases (and frequency decreases), primarily driven by residual dispersion.

4.4. Ultra-FRBs and propagation effects

Nimmo et al. (2022) and Snelders et al. (2023) discuss the detection of so-called ultra-FRBs, i.e., nanosecond to microsecond duration sub-bursts, from two repeating sources: FRB 20121102A and FRB 20200120E. Such extremely narrow sub-bursts warrant special attention

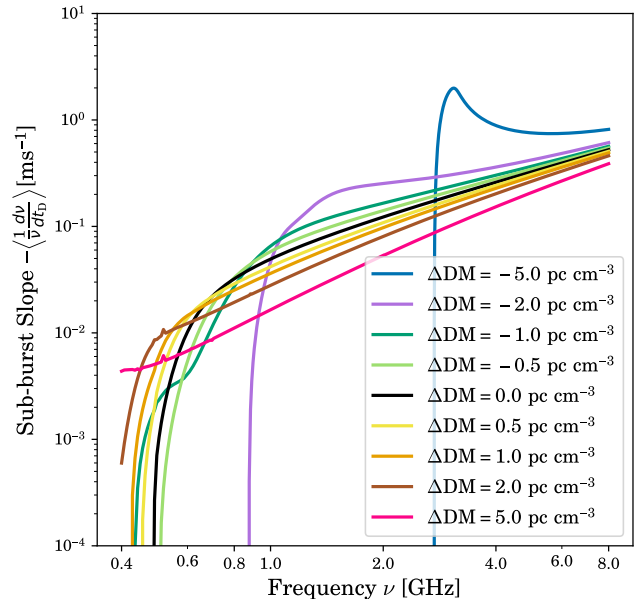


Figure 8. Same as Figure 7 but as a function of the center frequency. At high frequencies, the slope remains close to ideal except for severe over-dedispersion ($\Delta\text{DM} \approx 5.0$ pc cm^{-3}). Over-dispersed sub-bursts exhibit higher slopes, while under-dispersed sub-bursts display lower slopes. As frequency decreases, over-dispersed sub-bursts show erratic behavior due to the interplay with scattering effects.

due to their greater vulnerability to propagation effects, which can remain significant even at higher frequencies and shorter scattering timescales. Scattering influences both the duration and slope of sub-bursts, whereas residual dispersion primarily modifies the sub-burst slope. To study the effects of such distortions, we adjusted our parameters to simulate sub-bursts with durations of $50 \mu\text{s}$ at 1 GHz. The same analysis presented in Section 3.1 is then implemented to study the resulting sub-burst slope law.

For the scattering-only case, our findings for ultra-FRBs, represented by dotted lines in Figure 9, are juxtaposed against our previous analysis of 1.5 ms duration sub-bursts at 1 GHz (solid lines) to facilitate a comparative visualization. While the general behavior (as discussed in section 4.1.1) is similar for both ultra-FRBs and standard FRBs, the key distinction lies in their sensitivity to scattering. Ultra-FRBs (dotted lines) diverge from the ideal trend at shorter sub-burst durations compared to “standard” FRBs (solid lines) at all (non-zero) scattering timescales. This is due to their inherently shorter intrinsic durations, where even minimal scattering significantly smears the signal and alters the sub-burst slope. In other words, a small scattering-induced broadening that has a negligible effect on a millisecond-

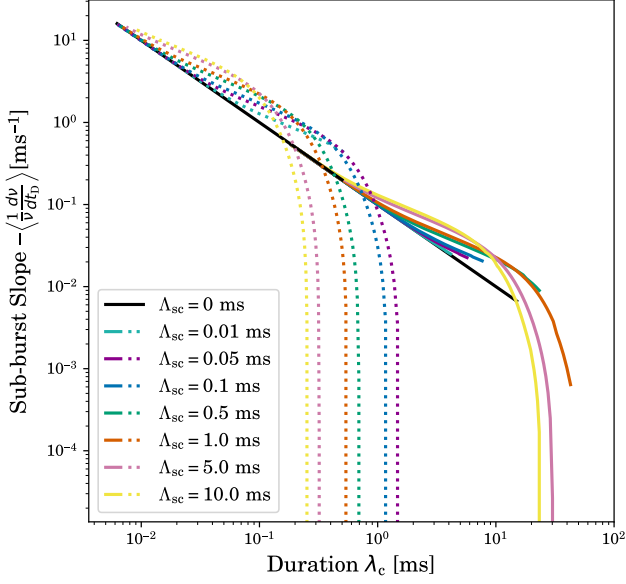


Figure 9. The (negative of the) normalized sub-burst slope as a function of duration with varying degrees of scattering for microsecond- and millisecond-duration sub-bursts. The solid black line represents the ideal sub-burst slope law in the absence of scattering. Solid colored lines correspond to millisecond-duration sub-bursts (i.e., 1.5 ms at 1 GHz), while dotted lines of the same colors represent microsecond-duration sub-bursts (i.e., 50 μ s at 1 GHz). The plot demonstrates that ultra-FRBs deviate from the ideal sub-burst slope law at shorter duration when subjected to the same scattering timescales.

duration sub-burst can completely dominate an ultra-FRB in view of its shorter duration.

In Figure 10, we present the (negative of the) normalized sub-burst slope (top plot) as well as duration (bottom plot) as functions of frequency for the ideal case without any propagation effects, comparing ultra-fast FRBs (dotted line) with standard FRBs (solid line). The significantly shorter durations of ultra-FRBs position them distinctly on duration-frequency plots, effectively forming a separate family of sub-bursts. Their durations are a factor of 30 (i.e., 1.5 ms/50 μ s) lower than the standard FRBs at all frequencies. At the same frequency, the sub-burst slope of ultra-fast FRBs is steeper. Despite these differences, both families follow the same sub-burst slope law (see Fig. 9), underscoring the robustness and universality of this relationship across different FRB populations.

In Figure 11, we present the sub-burst slope as a function of duration for ultra-FRBs for a restricted residual DM range of -0.2 pc cm^{-3} to 2.0 pc cm^{-3} . While the overall behavior resembles the trends discussed in section 4.2, we observe that smaller Δ DM values result in more pronounced deviations, at durations nearly two or-

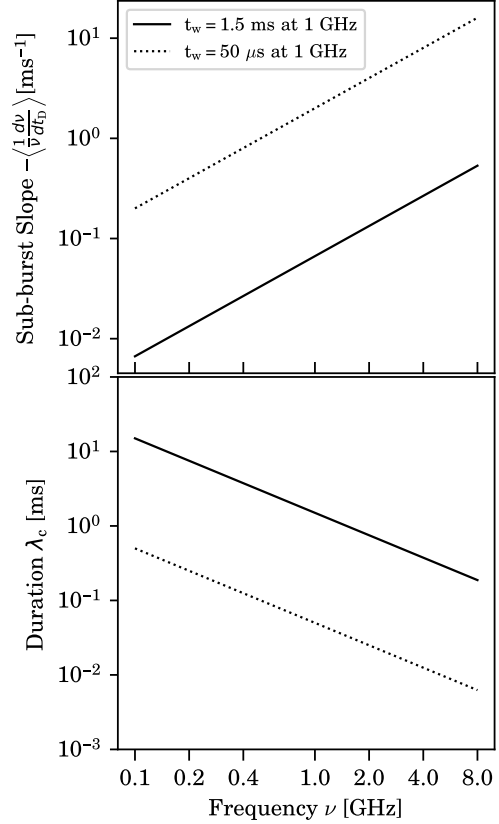


Figure 10. The (negative of the) normalized sub-burst slope (top panel) and duration (bottom panel) is plotted as a function of frequency for standard FRBs with a duration of 1.5 ms at 1 GHz (solid black line) and for ultra-FRBs with a duration of 50 μ s at 1 GHz (dotted black line). No propagation effects are present. A clear separation is seen between the two families of bursts.

ders of magnitude shorter compared to millisecond-long sub-bursts (see Figure 5). This heightened sensitivity to over-de dispersion is because ultra-FRBs already have a steeper intrinsic sub-burst slope in view of their extremely short durations, as expected from the sub-burst slope law (see equation 1). Overall, we find that all curves are shifted to the left (i.e., toward shorter durations).

These results underscore the level of precision required in correcting for scattering and dispersion for the measurement and analysis of ultra-FRBs. Even minimal residual dispersion or scattering can lead to erroneous sub-burst slope and duration measurements, resulting in misleading correlations between their properties. For example, one should avoid determining the DM of a source using ultra-FRBs unless measurements are performed at sufficiently high frequencies to minimize scattering effects.

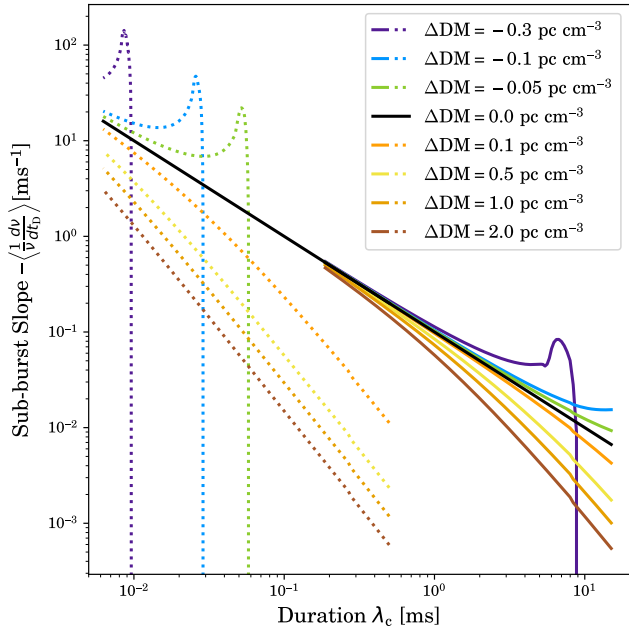


Figure 11. The sub-burst slope law as a function of frequency for microsecond- and millisecond-duration sub-bursts for $-0.2 \text{ pc cm}^{-3} \leq \Delta\text{DM} \leq 2.0 \text{ pc cm}^{-3}$. The solid black line represents the ideal sub-burst slope law in the absence of any residual dispersion. Solid colored lines correspond to millisecond-duration sub-bursts (i.e., 1.5 ms at 1 GHz), while dotted lines (following the same color scheme) represent microsecond-duration sub-bursts (i.e., 50 μs at 1 GHz). This plot illustrates that ultra-FRBs are highly sensitive to residual dispersion, with even minimal amounts of -0.2 pc cm^{-3} significantly affecting the sub-burst slope law.

5. SUMMARY

Through this study, we provide a comprehensive analysis of the impacts of scattering and residual dispersion on FRB spectra utilizing the TRDM. We begin by modeling sub-bursts with an intrinsic duration of 1.5 ms at 1 GHz, and later consider ultra-FRBs. Our numerical calculations reveal that scattering influences both the sub-burst slope and the duration of FRBs, with more pronounced effects at lower frequencies where longer scattering timescales are present. Although the effects can be dramatic for large scattering timescales (e.g., a change in the sign of the sub-burst slope; see Figs. 1 and 9), the absence of such behaviors in analyzed data (Rajabi et al. 2020; Chamma et al. 2021; Jahns et al. 2023; Chamma et al. 2023; Brown et al. 2024) suggests that the levels of scattering encountered in typical observations are relatively limited. Only subtle deviations are observed in Figures 3, 4, and 6 of Chamma et al. (2023) and Figures 1, 2, and 3 of Brown et al. (2024). At higher frequencies, the sub-burst dynamics align closely with the theoretical predictions of the TRDM, suggest-

ing a frequency-dependent scattering process underlying these observations. Our Figures 1, 3 and 4 parameterize the deviations induced by scattering, enabling quantitative comparisons with the observed trends. These plots provide a formal framework for interpreting subtle departures from idealized behavior, linking the observed deviations to underlying scattering effects with greater precision.

We then examine the effect of residual dispersion, uncovering distinct trends depending on whether the sub-burst is over-dedispersed or under-dedispersed. For moderate to weak over-dedispersion ($-1.0 \text{ pc cm}^{-3} \leq \Delta\text{DM} < 0 \text{ pc cm}^{-3}$), the sub-burst slope measured at shorter durations or higher frequencies closely resembles the undispersed case. However, excessive dedispersion of -2.0 pc cm^{-3} (and more negative values) forces the sub-burst slope to become extremely steep, causing the curve to lie markedly higher than the other cases. As the duration increases (or the central frequency decreases), the lower frequency components experience greater corrections to their arrival times as compared to the higher-frequency components. As a result, in cases of excessive over-dedispersion, the slope increases dramatically and eventually becomes positive. In under-dedispersed sub-bursts, the arrival times of lower-frequency components are increasingly delayed relative to those of higher-frequency components. This delay results in sub-burst slopes that are consistently lower than in the ideally dispersed case, with the deviations becoming more pronounced as ΔDM increases.

We then see the combined effects of dispersion and scattering on the sub-burst slope law. Over-dedispersion tends to increase the slope but scattering tends to decrease it. The interplay between these two effects produces the bumps observed in the sub-burst slope law of over-dedispersed bursts. In under-dedispersed sub-bursts, both effects work together in tandem to reduce the slope. Unlike scattering, residual dispersion prevents the slope from becoming completely flat or changing sign. Instead, these transitions are delayed to progressively longer durations, until scattering eventually dominates and dictates the curve's behavior.

In the case of ultra-FRBs, the effects of scattering and residual dispersion become more pronounced due to their extremely short timescales. In this analysis, we focus on sub-bursts with intrinsic durations of 50 μs at 1 GHz. Although the general behavior mirrors that of standard FRBs, the entire trend shifts toward shorter timescales and higher frequencies. Importantly, even weak scattering timescales and small residual dispersion introduce measurable distortions, impacting sub-bursts observed at frequencies that would typically be

regarded as high for standard FRBs. As a result, relying on these high-frequency bursts for DM estimation or analysis may lead to inaccuracies. Mitigating these distortions and achieving more precise measurements requires observations at even higher frequencies, where both scattering and residual dispersion effects are sufficiently suppressed for this class of sub-bursts.

The implications of this analysis are two-fold. First, we emphasize the importance of relying on high-frequency observations to accurately characterize the intrinsic properties and temporal structure of FRBs, thereby minimizing the effect of scattering. Second, although severe modifications in the sub-burst slope law are not observed in analyzed data, we caution that distortions caused by excessive scattering and residual dispersion could lead to misinterpretations of sub-burst properties, particularly in the case of ultra-FRBs. Departures from predicted behavior can serve as a warning

sign of the presence of complex interactions between the burst and propagation effects. Such deviations may also provide insights into the intrinsic mechanisms of FRBs and their interactions with their immediate environment, and the interstellar and intergalactic media. Our findings underscore the necessity of precise sub-burst pre-processing (e.g., determining accurate DMs) to mitigate the impact of frequency-dependent foreground processes.

ACKNOWLEDGMENTS

M.H.'s research is funded through the Natural Sciences and Engineering Research Council of Canada (NSERC) Discovery Grant RGPIN-2024-05242. F.R.'s research is supported by the NSERC Discovery Grant RGPIN-2024-06346.

REFERENCES

- Bethapudi, S., Spitler, L. G., Main, R. A., Li, D. Z., & Wharton, R. S. 2023, *MNRAS*, 524, 3303, doi: [10.1093/mnras/stad2009](https://doi.org/10.1093/mnras/stad2009)
- Brown, K., Chamma, M. A., Rajabi, F., et al. 2024, *MNRAS*, 529, L152, doi: [10.1093/mnras/lae012](https://doi.org/10.1093/mnras/lae012)
- Chamma, M. A., Rajabi, F., Kumar, A., & Houde, M. 2023, *MNRAS*, 522, 3036, doi: [10.1093/mnras/stad1108](https://doi.org/10.1093/mnras/stad1108)
- Chamma, M. A., Rajabi, F., Wyenberg, C. M., Mathews, A., & Houde, M. 2021, *MNRAS*, 507, 246, doi: [10.1093/mnras/stab2070](https://doi.org/10.1093/mnras/stab2070)
- Chawla, P., Kaspi, V. M., Ransom, S. M., et al. 2022, *ApJ*, 927, 35, doi: [10.3847/1538-4357/ac49e1](https://doi.org/10.3847/1538-4357/ac49e1)
- CHIME/FRB Collaboration, Amiri, M., Bandura, K., et al. 2019, *Nature*, 566, 230, doi: [10.1038/s41586-018-0867-7](https://doi.org/10.1038/s41586-018-0867-7)
- CHIME/FRB Collaboration, Andersen, B. C., Bandura, K., et al. 2023, *ApJ*, 947, 83, doi: [10.3847/1538-4357/acc6c1](https://doi.org/10.3847/1538-4357/acc6c1)
- CHIME/FRB Collaboration, Andersen, B. C., Bandura, K., Bhardwaj, M., et al. 2022, *Nature*, 607, 256, doi: [10.1038/s41586-022-04841-8](https://doi.org/10.1038/s41586-022-04841-8)
- Cordes, J. M., & Chatterjee, S. 2019, *ARA&A*, 57, 417, doi: [10.1146/annurev-astro-091918-104501](https://doi.org/10.1146/annurev-astro-091918-104501)
- Cordes, J. M., & Lazio, T. J. W. 2002, arXiv e-prints, astro, doi: [10.48550/arXiv.astro-ph/0207156](https://doi.org/10.48550/arXiv.astro-ph/0207156)
- Cronyn, W. M. 1970, *Science*, 168, 1453, doi: [10.1126/science.168.3938.1453](https://doi.org/10.1126/science.168.3938.1453)
- Farah, W., Flynn, C., Bailes, M., et al. 2019, *MNRAS*, 488, 2989, doi: [10.1093/mnras/stz1748](https://doi.org/10.1093/mnras/stz1748)
- Gajjar, V., Siemion, A. P. V., Price, D. C., et al. 2018, *ApJ*, 863, 2, doi: [10.3847/1538-4357/aad005](https://doi.org/10.3847/1538-4357/aad005)
- Gupta, V., Flynn, C., Farah, W., et al. 2022, *MNRAS*, 514, 5866, doi: [10.1093/mnras/stac1720](https://doi.org/10.1093/mnras/stac1720)
- Houde, M., Rajabi, F., Gaensler, B. M., Mathews, A., & Tranchant, V. 2019, *MNRAS*, 482, 5492, doi: [10.1093/mnras/sty3046](https://doi.org/10.1093/mnras/sty3046)
- Jahns, J. N., Spitler, L. G., Nimmo, K., et al. 2023, *MNRAS*, 519, 666, doi: [10.1093/mnras/stac3446](https://doi.org/10.1093/mnras/stac3446)
- Jankowski, F., et al. 2023, *MNRAS*, 524, 4275, doi: [10.1093/mnras/stad2041](https://doi.org/10.1093/mnras/stad2041)
- Kulkarni, S. R. 2020, arXiv e-prints, arXiv:2007.02886, doi: [10.48550/arXiv.2007.02886](https://doi.org/10.48550/arXiv.2007.02886)
- Nimmo, K., Hessels, J. W. T., Kirsten, F., et al. 2022, *Nature Astronomy*, 6, 393, doi: [10.1038/s41550-021-01569-9](https://doi.org/10.1038/s41550-021-01569-9)
- Ocker, S. K., Cordes, J. M., Chatterjee, S., et al. 2023, *MNRAS*, 519, 821, doi: [10.1093/mnras/stac3547](https://doi.org/10.1093/mnras/stac3547)
- Price, D. C., Foster, G., Geyer, M., et al. 2019, *MNRAS*, 486, 3636, doi: [10.1093/mnras/stz958](https://doi.org/10.1093/mnras/stz958)
- Rajabi, F., Chamma, M. A., Wyenberg, C. M., Mathews, A., & Houde, M. 2020, *MNRAS*, 498, 4936, doi: [10.1093/mnras/staa2723](https://doi.org/10.1093/mnras/staa2723)
- Ravi, V. 2019, *MNRAS*, 482, 1966, doi: [10.1093/mnras/sty1551](https://doi.org/10.1093/mnras/sty1551)
- Rickett, B. J. 1977, *ARA&A*, 15, 479, doi: [10.1146/annurev.aa.15.090177.002403](https://doi.org/10.1146/annurev.aa.15.090177.002403)
- Scheuer, P. A. G. 1968, *Nature*, 218, 920, doi: [10.1038/218920a0](https://doi.org/10.1038/218920a0)
- Shannon, R. M., Macquart, J. P., Bannister, K. W., et al. 2018, *Nature*, 562, 386, doi: [10.1038/s41586-018-0588-y](https://doi.org/10.1038/s41586-018-0588-y)

Snelders, M. P., Nimmo, K., Hessels, J. W. T., et al. 2023,
Nature Astronomy, 7, 1486,
doi: [10.1038/s41550-023-02101-x](https://doi.org/10.1038/s41550-023-02101-x)